Computation of the strong motions during the 1995 Hyogo-ken Nanbu earthquake, combining the k-square spectral source model and the discrete wavenumber technique.

C. Berge-Thierry, P. Lussou, B. Hernandez, F. Cotton & J.C Gariel
IPSN-DPRE-SERGD-BERSSIN, Fontenay-aux-Roses, France

ABSTRACT: We compute the strong ground motion at the 6 sites located in the Kobe Basin (KBU, KB1-4, RKI stations), using a stochastic spectral source description (Bernard et al., 1996), and the discrete wavenumber technique (Bouchon & Aki, 1977) in order to calculate complete field Green's functions in a *1D* medium. Such a model enables the generation of realistic (in temporal and spectral domains) broad-band strong motions. It is a numerical extended fault model. The rupture complexity is described by a specific seismic slip distribution, which has a k^{-2} spectral decay (k being the radial wavenumber). A rupture pulse propagates on the fault with a constant velocity, installing the dislocation. This model generates the standard frequencial ω^2 radiation for the accelerograms, as observed on the 1995 Kobe records, and allows to account for the directivity properties of the sources. The horizontal strong motion for the stations located in the basin is obtained by the convolution between the accelerogram evaluated at depth using the model described above and the non-linear transfer-function of the surrounding sediments (computed by a non-linear code called CyberQuake). The frequency validity domain of our synthetics is 0.1 to 4 *Hz*.

1 INTRODUCTION

We propose to simulate the strong motion due to the 1995 Kobe earthquake using a totally numerical method. This method has been developped in order to assess the seismic motion in area of low and moderate seismicity, where the data are not available or to scattered in location and magnitude. Recently, Herrero & Bernard (1994) proposed a simple kinematic model of earthquake rupture that produces broad-band seismograms with a ω^{-2} decay of displacement spectrum. The originality of the model lies in the dislocation distribution which is self-similar and has a k^{-2} decay in the wavenumber space. Such k^{-2} dislocations enable the generation of realistic accelerograms with a ω^0 high-frequency level. One advantage of this model is the ability to generate strong-motion accelerograms for nearby sources, i.e. closer than the length of the seismic source. Furthermore, physical characteristics of the source, such as stress drop or directivity effect that are generally not introduced in statistical methods, are taken into account in this model. The directivity properties of the source are modelled considering a propagating pulse associated to a specific spectral source time function (Bernard et al., 1996). Instead of the far field term of the radiation computation, as proposed by Herrero and Bernard (1994) and Bernard et al. (1996), we compute here the numerical Green's functions using the discrete wavenumber technique developped initially by Bouchon and Aki (1977), and adapted by Coutant (1997). Consequently we obtain *1D* Green's functions for the complete wave field. Finally, we consider the non-linear transfer function for the stations located above the sedimentary basin (ie, for all the sites excepted KBU, which is considered to be on rock-site) in order to calculate the horizontal acceleration.

2 THE SPECTRAL SOURCE MODEL

In the following section, we present the hypothesis of our model. The spatial description of the source and the temporal history of the rupture are described.

2.1 *Principes of ground-motion calculation*

The source geometry is modeled by 3 rectangular fault planes discretized in many subfaults whose number depends on the maximum frequency under consideration. The Green's functions are computed using the discrete wavenumber technique in a *1D* medium specified for each site. KBU is a rock- site, its accelerogram is evaluated at the surface directly using only the elastic response of the medium, whereas the 5 others stations are considered to be at depth (at 20.5 *m* for KB1, 20. *m* for KB2, 34.1 *m* for KB3, 30.2 *m* for KB4 and 110 *m* for RKI): the effect of the surrounding sediments on horizontal motion

is accounted by the transfer function computed using the non-linear CyberQuake code (Brgm, 1998). Within each subfault, the Fraunhaufer approximation is made and directivity appears through the standard directivity term C_d (see Herrero and Bernard, 1994). Each sub-fault has a final dislocation value, and the global dislocation distribution takes place on the fault with a propagating pulse, associated to a specific source-time function. The spatial location of the fault is given on Figure 1.

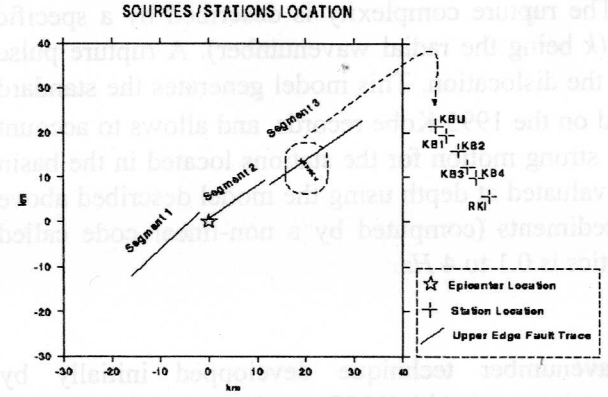

Figure 1: Location of the 3 segments of the fault and stations.

2.2 *The dislocation distribution properties*

The broad-band characteristic of the radiated strong motion is given by the complexity of the dislocation distribution. The number of sub faults on the fault plane implies the maximal frequency of the modeling. The dislocation has a k^{-2} spectral shape, k being the radial wavenumber. The low wavenumber component of the dislocation is deterministic and linked to the length of the fault, whereas the high wavenumber part is stochastic. Herrero & Bernard (1994) showed that such a dislocation enables the computation of strong-motions, that have the standard ω^2 radiation. For the Kobe specific case, we simulate the main shock considering three fault planes, named segment 1 (Nojima fault), segment 2 (Suma and Suwayama faults) and segment 3 (Gosukebashi fault). The dimensions and focal mechanism of each segment are given in Table 1: all these values have been chosen considering papers and results of several studies.

Table1: Physical properties of the 3 segments.

	Length (km)	Width (km)	Strike (deg)	Dip (deg)	Slip (m)	Δu (m)
Seg1	20	20	45	82	180	1.17
Seg2	15	20	53	90	180	0.44
Seg3	24	20	233	89	180	0.32

The dislocation on each segment has been composed in order to respect the location of the main asperities defined by inversion method results (as in Sekiguchi et al., 1996). Mean dislocation on each segment has been deduced from Sekiguchi et al. (1996) moment distribution results. Each segment has been discretized in 128 x 128 subfaults, allowing a 4 Hz maximal frequency for the modelling. Dislocation distributions used to simulate the strong ground motions during the Kobe earthquake are presented on Figure 2.

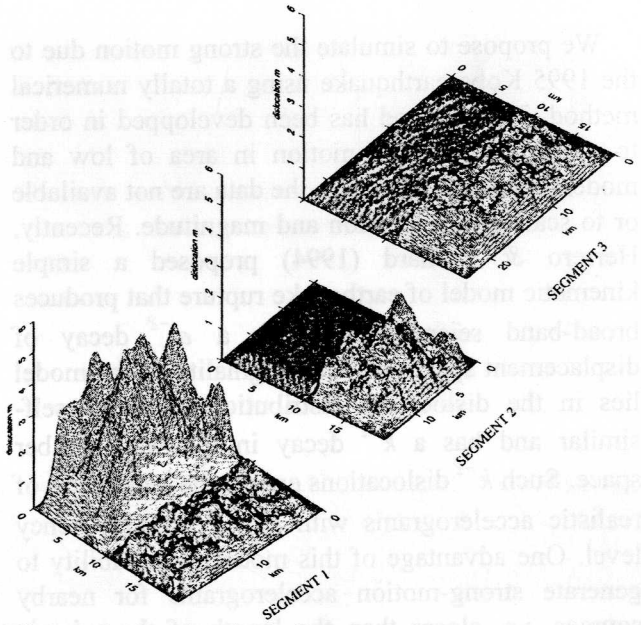

Figure 2: Stochastic k^{-2} dislocation distribution for each segment of the Kobe earthquake. Mean dislocation values and asperities locations have been determined after inversion results (Sekiguchi et al., 1996).

2.3 *Directivity properties of the model*

The second originality of the model is the wavenumber dependent source time function.

The complexity of this rise time has been introduced in our model, in order to avoid the classical Cd^2 amplification, due to an instantaneous dislocation (i.e, a quasi Heaviside rise time), Cd being the directivity factor (linked to the rupture velovity, and the θ angle between the ray path and the source to receiver azimuth). The propagating pulse (Haskell type or Circular) has a constant width (L_0 and propagates with a constant rupture velocity (V_r = 2.8 km/s in the Kobe modelling). The source time-function is defined in the radial wavenumber space, as

$$\tau_k = L_0 / V_r = \tau_{max} , k < 2\pi a / L_0 \qquad (1)$$

$$\tau_k = \tau_{max} * 2\pi a / L_0 * 1 / k , k > 2\pi a / L_0 \qquad (2)$$

where L_0 is the width of the pulse, V_r the rupture velocity, k the radial wavenumber and a is a constant of about 1. The combination of the propagating pulse and the spectral source time function allows to reduce the non realistic Cd^2 amplification. A parametric study is detailed in Bernard et al., 1996, in which the effects of the width of the pulse, the rupture velocity on the radiated motion are presented, with respect to the source to receiver directivity configuration. The numerical implementation of this method is presented in Berge et al. (1998). To summarize, the propagating pulse concept, associated to the k^{-2} dislocation, and the wavenumber source time function allows to generate realistic ω^2 accelerograms, including directivity properties. For the Kobe simulation, we consider a circular pulse for segment 1 and segment 2, and a rectilinear one (Haskell type) for the third segment. The nucleation of the rupture is located on the northern limit of the first segment (at 17 *km* at depth) (and corresponds to the southern border of the second segement, as described in Sekiguchi et al., 1996). The radiation due to the third segment is computed considering an Haskell pulse initiated at the soutern extremity of the fault (in the width of the plane). The final seismogram is obtained by summation of the synchrone contributions of the first and second segments, whereas the contribution of the third segment has been dephased in time (of the rupture propagation time on the second segment). The width of the propagating pulse has been determined after Sekiguchi et al. (1996) rise time distribution results. We calculated the averaged rise time (1.2 *s*) on the whole plane defining in this way the τ_{max} value of our model (see equations (1) and (2)). We then obtained a 3360 *m* width for the pulse.

3 GREEN'S FUNCTIONS COMPUTATION

For generating the numerical Green's functions, we used the wavenumber technique of Bouchon and Aki (1977) and coupled it to the reflection coefficient propagator method of Kenett and Kerry (1979). We do not evaluate the Green's function at each source point of the 3 segments: for each segment, we compute completely the Green's function for 1156 source points located on the whole plane (and surrounding it, as presented on Figure 3), and we obtain the Green's functions for the 128 *x* 128 real positions by an interpolation method. Our interpolation method is based on the one of Lachet (1996), modified to account for only the fourth nearest computed Green's functions. This interpolation notably decreases the time computation.

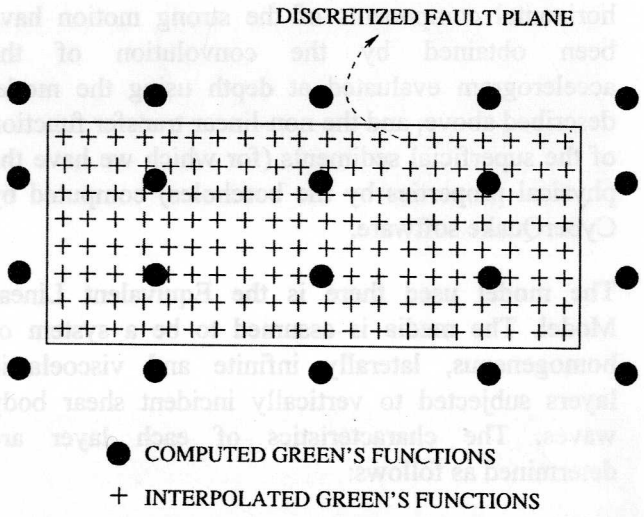

Figure 3: Location of the computed (black circles) and interpolated (crosses)Green's functions.

The *1D* velocity structures considered for each site are described in Tables 2, 3, and 4 of Annexe 1 (see Iwata et al., 1996). The velocity structure at KBU has been modified, considering a 20 *m* thick weathered layer.

The 3 components of the strong motion at KBU are computed using the standard procedure described above, considering the physical properties of Table 2.

The horizontal components of KB1, KB2, KB3, KB4 and RKI strong motions are evaluated at depth, using the physical properties of Tables 3 and 4. The physical characteristics of surrounding sediments at these 5 stations are described in Tables 5, 6, 7, 8, and 9 of Annexe 2.

The vertical component of the strong motion at KB1, KB2, KB3, KB4 and RKI is computed using the standard procedure (i.e the station being located at 0 *m* at depth), considering velocity model which includes the superficial soft sediments (physical parameters presented in Tables 10, 11, 12, 13 and 14 of Annexe 3, avereged from values of Annexe 2). We do not compute the vertical component with the non-linear code, because the vertical incidence of the input signal do not allow to model the surface waves. We thus consider the vertical component to be much well synthetized by the complete wavefield computation up to the ground surface.

4 NON-LINEAR TRANSFER FUNCTION COMPUTATION

For the KB1, KB2, KB3, KB4 and RKI sites, the horizontal components of the strong motion have been obtained by the convolution of the accelerogram evaluated at depth using the model described above, and the non-linear transfer function of the superficial sediments (for which we have the physical properties by the boreholes) computed by CyberQuake software.

The model used there is the Equivalent Linear Model. The media is assumed to be a system of homogeneous, laterally infinite and viscoelastic layers subjected to vertically incident shear body waves. The characteristics of each layer are determined as follows:

- the STP N-vallues are translated into S-wave velocity with the Ohta and Goto's formula : $Vs=68.70*N^{0.171}*H^{0.189}*E*F$ given in the readme file of ESG.

- a G-gamma curve and a D-gamma curve are associated with each layer. Thoses curves are deducted form soil structure and litterature (Seed and Idriss, 1970, Seed et al., 1986, Vucetic and Dobry, 1991).

- density is estimated from soil structure and depth.

The two horizontal components of motion are taken into account separatly,the apparent shear modulus of each direction is assumed to varie with the absolute value of the shear strain in this direction. The damping is assumed to be frequency independent.

5 CONCLUSIONS

As conclusion, we present the comparison between our synthetics and data for KBU and RKI. Data and synthetics are both filtered between 0.1 to 4 *Hz*, and the acceleration is plotted (figures 4 and 5).

A comparison of the spectra is thus presented on same figures.

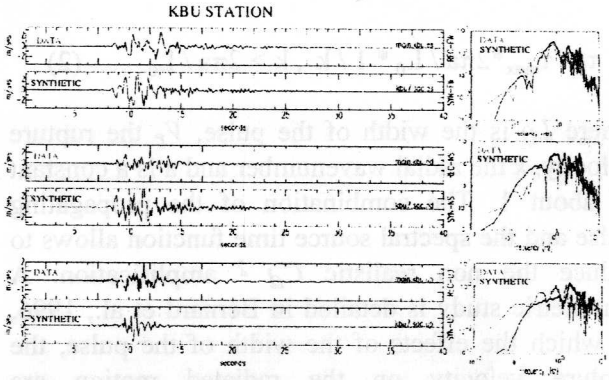

Figure 4: Comparison between data (top) and synthetic (bottom) for the 3 components (east, north and up) of the acceleration at KBU site. On the right of the picture is plotted the corresponding spectra.

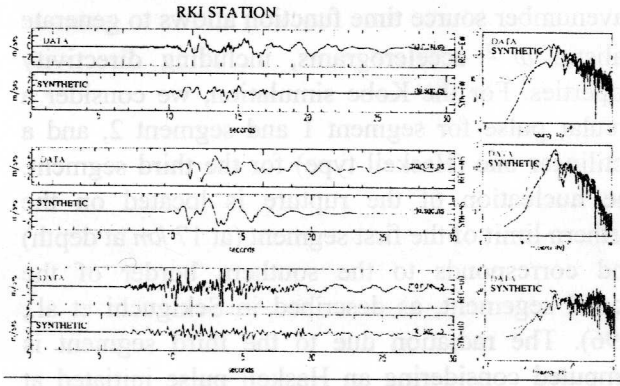

Figure 5: Comparison between data (top) and synthetic (bottom) for the 3 components (east, north and up) of the acceleration at RKI site. on the right of the picture is plotted the corresponding spectra. For this station, the horizontal components are computed taking account for the non-linearity of the surroundinf soft sediments.

On the figures 4 and 5, we observe a good fit between data and synthetics on the whole frequency range of the modelisation (0.1 to 4 *Hz*). The lack at some specific frequencies could be explain by the pure 1D modelling.

The method is thus satisfaying in term of temporal signal form prediction, as in frequencial content. The modeling of non-linear phenomena using the CyberQuake software (Brgm, 1998) allows to obtain realistic seismograms, as illustrated on Figure 5. The knowledge of the velocity structure appears very important in our *1D* modeling, in order the generate good Peak Ground Acceleration values and 3 components realistic modellings. That is for example the reason we have introduced a weathered layer for the KBU site velocity model, in order to generate a vertical component with an amplitude comparable to the horizontal one.

Such a model is really interesting in seismic hazard assessment for strong motion prediction. The *1D* approach is often a good first approximation of the velocity structure in our geological context. The modeling of the complete wave field appears very important, in order to synthetize all the phases, especially the crustal and surface waves.

In term of time computation, for example to generate the 3 components of the motion for 1 station (using the Kobe case, i.e, 3 segments discretized in 128 *x* 128 sub-faults, computing a 60 *s* seismogram with a maximal frequency of 4 *Hz* and interpolation of the Green's functions): using a DEC machine (EV5-300*MHz*) with 2 *Go* of memory, we need less about 1 hour and half per station. This time computation seems quite reasonnable because it is a complex broad band source simulation, with a complete wave field computation.

The association of our complex source with a complete *3D* wave propagation is the next step of our our work.

REFERENCES

Berge C., J.C. Gariel, and P. Bernard, A very broad-band stochastic source modelfor near source strong motion, *Geoph. Res. Letters*, Vol. 25, No. 7, 1998.

Bernard, P., A. Herrero, and C. Berge, 1996, Modeling Directivity of Heterogeneous Earthquake Ruptures, *Bull. Seis. Soc. Am*, Vol. 86, No. 4, 1196.

Bouchon, M. and K. Aki 1977, Discrete wave-number representation of seismic-source wave fields, *Bull. Seism. Soc. Am.*, Vol. 67 , No. 2, 1977.

Coutant, O., Programme de simulation numerique Axitra, LGIT, Universite Grenoble I, 1997.

CyberQuake, a Software from The Bureau de Recherches Geologiques et Minieres, BRGM, 1996-1998, France.

Herrero, A., and P. Bernard, 1994, A kinematic self-similar rupture process for earthquakes, *Bull. Seis. Soc. Am.*, Vol. 84, 1994.

Iwata T., H. Sekiguchi, K. Hatayama and A. Pitarka, Generation of strong ground motions during the 1995 Hyogo-ken Nanbu earthquake in Kobe area - source and site effects, *Book entitled ' Strong motion seismology, Lesson from the 1995 Hyogo-ken Nanbu earthquake'*, Edited by K. Irikura, T. Iwata and H. Sekiguchi, pp 479-509, 1994-1998.

Kennett B.L.N. and N.J. Kerry, Seismic waves in a stratified half space, Geophys. *J. R. Astr.*, Vol. 57, 1979.

Lachet C., Observation des s\'eismes en milieux urbains: Methodes simples d'etude des effets de site et de simulation des mouvements forts, *Ph.D Thesis*, Universite Grenoble I, 1996.

Seed, H.B. and I.M. Idriss, Soil Moduli and domaping factors for dynamic response analysis of horizontally layered sites, Report No UCB/EERC 70-10, Earthquake Engineering Research Center, University of California, Berkeley, CA, 1970.

Seed, H.B., Wong, R.T., Idriss, I.M. and Tokimatsu, K. Moduli and damping factors for dynamics analyses of cohesionless soils , *Journal of Geotechnical Engineering*, ASCE, Vol. 112 (11), 1016-1032, 1986.

Sekiguchi, H., K. Irikura, T. Iwata, Y. Kakehi and M. Hoshiba, Minute locating of faulting beneath Kobe and the waveform inversion of the source process during the 1995 Hyogo-ken Nanbu, Japan, earthquake using strong ground motion records, *J. Phys. Earth.*, Vol. 44, 1996.

Vucetic, M. and R. Dobry Effect of soil plasticity on cyclic response, *Journal of Geotechnical Engineering*, ASCE, Vol.117 (1), 89-107, 1991.

ANNEXE 1

The geological structures described in these 3 tables have been used to compute the 3 components at KBU (at depth = 0 m), and to calculate the horizontal components for RKI, KB1, KB2, KB3 and KB4 evaluated respectively at 110 *m*, 20.5 *m*, 20. *m*, 34.1 *m* and 30.2 *m* at depth: these horizontal seismograms evaluated at depth being the inputs of the non-linear process.

Table 2: Soil characteristics for KBU.

Interf. Depth (m)	Vp (m/s)	Vs (m/s)	ρ (kg/m^3)	Qp	Qs
0	2200	1200	1800	150	40
20.	3200	1800	2100	400	200
400.	5150.	2850.	2500	500	200
550	5500	3200	2600	550	300
5000	6000	3460	2700	900	400
18000	6700	3870	2800	1200	500

Table3: Soil characteristics for KB1 and KB2.

Interf. Depth (m)	Vp (m/s)	Vs (m/s)	ρ (kg/m^3)	Qp	Qs
0	1600	400	1700	150	40
400.	2500	1000	2200	350	100
800.	4250.	2850.	2300	400	150
5000	6000	3460	2800	1300	600
18000	6700	3870	2800	1200	500

Table 4: Soil characteristics for KB3, KB4 and RKI.

Interf. Depth (m)	Vp (m/s)	Vs (m/s)	ρ (kg/m^3)	Qp	Qs
0	1400	100	1400	50	20
20.	1600	400	1800	200	50
450.	2500.	1000.	2200	350	100
900	4250	2850	2300	400	150
5000	6000	3460	2800	1300	600
18000	6700	3870	2800	1200	500

ANNEXE 2

These 5 tables describe the geological structures and physical parameters used in the Cyberquake code in order to compute the non-linear transfer function of surrounding soft sediments at KB1, KB2, KB3, KB4 and RKI stations. These transfer functions have been applied on horizontal components only. These values have been defined after the informations given in the guidelines (borehole description). The symbol & seems that for example clay & silt are in an equal proportion, whereas the symbol - significates that sand dominates in a sand - gravel material.

Table 5: Surrounding layers at KB1.

	Deposit Type	Thickness (m)	Vs (m/s)	ρ (kg/m^3)
layer 1	Surface deposit	0.5	150	1500
layer 2	Sand	3.8	150	1500
layer 3	Sand & Gravel	1.6	250	1500
layer 4	Gravel	0.6	275	1500
layer 5	Sand	1.1	200	1600
layer 6	Sand & Clay	0.8	200	1600
layer 7	Sand	3.1	225	1600
layer 8	Sand & Clay	1.1	225	1700
layer 9	Sand	3.5	250	1700
layer 10	Sand & Gravel	4.1	325	1800
layer 11	Sand	0.3	250	1800
Bedrock	Bedrock	infinite	1500	2400

Table 6: Surrounding layers at KB2.

	Deposit Type	Thickness (m)	Vs (m/s)	ρ (kg/m^3)
layer 1	Sand	3.0	150	1500
layer 2	Sand & Gravel	2.9	200	1500
layer 3	Gravel	0.2	250	1500
layer 4	Sand - Gravel	1.0	200	2000
layer 5	Silt	0.2	200	1600
layer 6	Sand & Gravel	2.3	275	1600
layer 7	Sand & Gravel	4.5	300	1800
layer 8	Sand & Gravel	5.9	300	1800
Bedrock	Bedrock	infinite	1500	2400

Table 7: Surrounding layers at KB3.

	Deposit Type	Thickness (m)	Vs (m/s)	ρ (kg/m^3)
layer 1	Soil Deposit	6.6	150	1500
layer 2	Sand	3.4	200	1500
layer 3	Sand & Silt	2.5	175	1600
layer 4	Sand - Gravel	3.0	225	1600
layer 5	Sand & Silt	1.3	200	1600
layer 6	Sand	1.1	250	1700
layer 7	Sand & Gravel	4.5	300	1800
layer 8	Sand & Gravel	5.0	350	1800
layer 9	Sand	5.5	260	1800
layer 10	Sand & Gravel	2.0	375	2000
layer 11	Sand & Gravel	2.0	275	2000
Bedrock	Bedrock	infinite	2085	2600

Table 8: Surrounding layers at KB4.

	Deposit Type	Thickness (m)	Vs (m/s)	ρ (kg/m^3)
layer 1	Soil Deposit	18.6	150	1500
layer 2	Silt	3.0	150	1600
layer 3	Sand	1.1	216	1800
layer 4	Silt	0.8	185	1800
layer 5	Sand-Gravel	6.7	265	2000
Bedrock	Bedrock	infinite	2085	2600

Table 9: Surrounding layers at RKI.

	Deposit Type	Thickness (m)	Vs (m/s)	ρ (kg/m^3)
layer 1	Gravel & Sand	3.5	175	1900
layer 2	Sand & Gravel	3.0	175	1900
layer 3	Sand & Gravel	6.0	200	1900
layer 4	Sand & Gravel	5.0	200	1900
layer 5	Sand & Gravel	3.0	250	1900
layer 6	Clay & Silt	10	200	1650
layer 7	Clay & Silt	4.5	220	1700
layer 8	Sand & Gravel	11.	380	1800
layer 9	Sand & Gravel	24.	340	1900
layer 10	Clay & Silt	20.	270	1600
layer 11	Sand & Gravel	10.	430	1900
layer 12	Clay & Silt	5.0	350	1700
Bedrock	Bedrock	infinite	3800	2500

ANNEXE 3

These 5 tables describe the velocity models used to compute the vertical component at KB1, KB2, KB3, KB4 and RKI stations. For the computation of the vertical component the stations are supposed to be at depth 0 m.

Table 10: Soil characteristics for KB1: vertical component only.

Interf. Depth (m)	Vp (m/s)	Vs (m/s)	ρ (kg/m^3)	Qp	Qs
0	1050	150	1500	150	40
4.3	1500	260	1500	200	50
6.5	1200.	200.	1600	200	50
8.4	1350	250	1750	250	50
20.5	2500	1000	2200	35	100
800	4250	2850	2300	400	150
5000	6000	3460	2800	1300	600

Table 11: Soil characteristics for KB2: vertical component only.

Interf. Depth (m)	Vp (m/s)	Vs (m/s)	ρ (kg/m^3)	Qp	Qs
0	1050	150	1500	150	40
21.6	1500	200	1800	200	50
23.5	2500.	265.	2000	300	100
30.2	4250	2850	2300	400	150
20.5	2500	1000	2200	35	100
5000	6000.	3460	2800	1300	600
18000	6700	3870	2800	1200	500

Table 12: Soil characteristics for KB3: vertical component only.

Interf. Depth (m)	Vp (m/s)	Vs (m/s)	ρ (kg/m^3)	Qp	Qs
0	1050	170	1500	200	50
10.	1200	220	1600	200	100
18.4	1550	300.	1800	200	100
28.9	2500	350	2000	350	100
34.1	4250	2085	2600	400	150
900	4250	2850	2300	400	150
5000	6000	3460	2800	1300	600
18000	6700	3870	2800	1200	500

Table 13: Soil characteristics for KB4: vertical component only.

Interf. Depth (m)	Vp (m/s)	Vs (m/s)	ρ (kg/m^3)	Qp	Qs
0	1050	150	1500	200	50
21.6	1500	200	1800	200	50
23.5	2500	265	2000	350	100
30.2	4250	2085	2600	400	150
34.1	4250	2085	2600	400	150
900	4250	2850	2300	400	150
5000	6000	3460	2800	1300	600
18000	6700	3870	3000	1700	800

Table 14: Soil characteristics for RKI: vertical component only.

Interf. Depth (m)	Vp (m/s)	Vs (m/s)	ρ (kg/m^3)	Qp	Qs
0	825	187.5	1900	100	50
16.5	1360	220	1800	150	50
50	1365	315	1750	150	50
30.2	4250	2085	2600	400	150
105	1400	400	1850	200	100
450	2500	1000	2200	350	100
900	4250	2850	2300	400	150
5000	6000	3460	2800	1300	600
18000	6700	3870	3000	1700	800